MoO$_3$ incorporation in magnesium aluminosilicate glasses

Shengheng Tan, Michael I Ojovan, Neil C Hyatt and Russell J Hand

ISL, Department of Materials Science & Engineering, University of Sheffield, Sir Robert Hadfield Building, Mappin Street, Sheffield, S1 3JD, UK

Abstract

Molybdate has a very low solubility in silicate and borosilicate glass systems and its excess presence in nuclear waste glass can cause the formation of a readily soluble "yellow phase". In this study, the incorporation of molybdenum oxide (MoO$_3$) in a magnesium aluminosilicate glass system has been investigated. The prepared glasses show a higher than 90% molybdenum retention rate and up to 5.34 mol% (12.28 wt%) MoO$_3$ can be incorporated into these glasses without causing visible phase separation. The incorporation of MoO$_3$ increases glass density, decreases glass transition and crystallisation temperatures and intensifies Raman bands assigned to vibrations of MoO$_4^{2-}$ units. When excess molybdate is added liquid-liquid phase separation and crystallisation occurs. The separated phase is spherical, 200-400 nm in diameter and randomly dispersed. Based on powder X-ray diffraction, Raman spectroscopy and transmission electron microscopy, the separated phase is identified as MgMoO$_4$.

Introduction

Some of the high level nuclear waste (HLW) produced in the UK and France contains a high concentration of MoO_3 [1-2], one of the most challenging oxides occurring in the vitrification of radioactive wastestreams on account of its low solubility (≤ 1 wt%) in the conventionally used borosilicate glasses [3]. MoO_3 at higher levels in nuclear waste glasses can cause the formation of "yellow phase" (a mixture of alkali and alkaline earth molybdates with chromates and sulphates) [4-5], which is detrimental to HLW vitrification process. The yellow phase not only accelerates the corrosion of the melter but also reduces the performance of the vitrified product since it can contain problematic radionuclides (e.g. ^{137}Cs) and can be dissolved if it comes into contact with water [6-8]. Therefore, the waste loading capacity for Mo-rich wastes in vitrification has been restricted to avoid the formation of yellow phase. However, post-operational clean-out wastes from Sellafield in the UK and some French wastes (e.g. [2]) contain high levels of MoO_3 hence identifying glass composition with high MoO_3 compatibility is desirable.

Many studies have been undertaken to understand molybdate incorporation and to improve molybdate solubility in silicate glasses. Mo predominantly occurs as a hexavalent state Mo^{6+} in glasses prepared under oxidising and neutral atmospheres, regardless of glass composition [9-10] with each Mo^{6+} cation being coordinated with four oxygens to form a MoO_4^{2-} tetrahedron. The average Mo-O distance range is 1.76-1.78 Å, indicating that Mo^{6+} has a high field strength range of 1.89-1.94 Å^{-2} in glass [6, 10-13] and thus Mo^{6+} cations have a strong ordering effect on surrounding oxygens [14]. Consequently, the MoO_4^{2-} tetrahedra can be easily separated from the silicate glass network. Meanwhile, it has been observed that MoO_4^{2-} ions are preferentially associated with the network modifying cations [12] and are thus located in alkalis and alkaline earth enriched domains in glass network [11]. MoO_4^{2-} tends to form alkali or alkaline earth molybdate crystals on separating out from the glass network and therefore the molybdate solubility can be related to the cations with which the MoO_4^{2-} tetrahedra are associated. Tailoring glass composition so as to improve molybdate solubility in borosilicate glasses has been undertaken by a number of workers [2, 14-17]; however, the solubility is still low. For example, Caurant and co-workers [14, 17] have found that increasing the B_2O_3 level in a Ca-Na borosilicate glass, which is supposed to consume more Na^+ cations thereby enabling more MoO_4^{2-} units to be connected with Ca^{2+}, does not enhance molybdate capacity in glass in reality. Instead, the crystallisation of Na_2MoO_4 becomes less favourable.

To the best of our knowledge, little attention has been paid to molybdate incorporation and solubility in aluminosilicate glasses, even though such glasses have been investigated as formulations for nuclear waste vitrification since the late 1950s in Canada [18]. Aluminosilicates have good glass formation ability, high chemical durability and thermal stability [19-23], however applications of these glasses have been limited by their high melting temperatures and low waste loading capacities [18]. Recent studies [24-25] indicated that calcium aluminosilicate glasses are able to accommodate a large quantity of chlorine. Given that molybdenum and chlorine are both present as anions (MoO_4^{2-} and Cl^-), poorly soluble and only associated with network modifiers in silicate glass, it was considered to be worth investigating molybdate solubility in aluminosilicate glass compositions.

Our preliminary work shows that magnesium aluminosilicate (MAS) glass possesses the highest MoO_3 solubility among all alkaline earth (Mg to Ba) aluminosilicate glasses

investigated. In this paper, the capacity of MAS glass networks to accommodate molybdate, the influence of molybdate incorporation on the glass structure and properties, as well as the phase separation caused when the solubility limit of molybdenum is exceeded in the glass are assessed.

2. Experimental

2.1. Glass making

A series of MAS glasses ($45SiO_2$-$10Al_2O_3$-$45MgO$, mol%) with different MoO_3 additions (0-8 mol%) were produced. The nominal compositions of these glasses are listed in Table 1. The reagents to produce glass batches include high purity glass making sand (SiO_2, Loch Aline sand, Tilcon, UK), aluminium trihydroxide ($Al(OH)_3$, Acros Organics, UK), magnesium hydroxide ($Mg(OH)_2$, Sigma Aldrich, UK) and molybdenum trioxide (MoO_3, Sigma Aldrich, UK). All reagents are of laboratory purity. Batches to produce ~50 g glass were placed in mullite crucibles. The glass batches were heated in an electric furnace from room temperature to 1450 ℃ at 2 ℃ min^{-1}, held for 3 h and afterwards poured out into a preheated steel mould to form a block. The cast glass was immediately transferred to another electric furnace where it was annealed at 700 ℃ for 1 h and cooled down to room temperature at 1 ℃ min^{-1}. All of the above procedures were carried out in air.

2.2. Sample characterisation

The density of glasses was determined with a Mettler Toledo densimeter which is based on Archimedes principle using deionised water as the medium (measurement precision 0.001 g cm^{-3}). The density was measured for each sample was repeated five times and the average result taken.

The thermal behaviours of the prepared glasses were investigated by differential thermal analysis and thermogravimetric analysis (DTA & TGA, Perkin Elmer 7). Sample powders passing a 75 µm sieve were collected for use. Samples were placed in a platinum crucible and heated from room temperature to 1000 ℃ at 10 ℃ min^{-1} using an equivalent weight of alumina as the inert reference. The amorphous nature of the glasses or any separated phase in inhomogeneous samples were confirmed or identified by X-ray diffraction (XRD) using a Siemens D5000 powder diffractometer, with Cu-Kα radiation operating at 40 kV and 40 mA, over a 2θ range of 10-60° with 0.05° step size and 7 s dwell time. High temperature XRD (HT-XRD) was performed in a Siemens HT-D5000 powder diffractometer with the same settings as the room temperature XRD except that the dwell time was 10 s. In this case diffraction patterns were recorded at 30, 850, 900, 950 and 1000 ℃, with a heating rate of 10 ℃ min^{-1}. A final scan at 30 ℃ was performed on the quenched sample. In both XRD and HT-XRD powdered samples with a particle size of <75 µm were used. Crystalline phase identification was undertaken using the PDF4 (2012) database produced by the International Centre for Diffraction Data (ICDD).

For Raman spectroscopy the glass bars were cut into slices ~5 mm thick using a Buehler low speed saw with a diamond blade and with oil as lubricant. The top surfaces of the slices were ground to 1200 SiC grit, rinsed with isopropanol and thoroughly dried. Raman spectra were recorded with a Renishaw Invia Raman spectrometer equipped with a CCD detector, using a green line (514.5 nm) laser at 20 mW laser power and a ×50 objective. The energy range 0 - 2000 cm^{-1} was scanned, with a resolution of 1 cm^{-1} and exposure time of 10 s. 10 spectra were accumulated for each sample. Calibration with silicon was undertaken each time the spectrometer was used.

The morphology and microstructure of samples were examined by scanning electron microscopy (SEM) and transmission electron microscopy (TEM). SEM observation was performed in an FEI Inspect F microscope using both secondary electron imaging (SEI) and backscattered electron imaging (BEI). Glass compositions were determined

by an energy dispersive X-ray spectrometer (EDS, INCA Oxford Instruments) attached to a JEOL JSM6400 SEM. Calibration with cobalt was undertaken for each sample and the estimated error in the major components is $\leq 1\%$. The measured glass compositions are listed in Table 1 in comparison with the nominal glass compositions. In addition, elemental distribution was investigated by X-ray mapping within an area of 1600 μm^2 in glass during EDS analysis. Specimens for SEM and EDS were prepared by mounting glass slices into epoxy resins, grinding to 1200 SiC grit and polishing to 1 µm with diamond suspension. The prepared specimens were coated with carbon and painted with silver paste before analysis. TEM observation was carried out in a Philips EM420 microscope at 120 kV. Specimens for TEM were prepared by grinding the crushed sample pieces with acetone in an agate mortar and pestle for 20 min. One drop of the resulting suspension was loaded to a holey carbon-filmed copper grit for TEM observation.

3. Results

3.1. Molybdate solubility and retention

Molybdate incorporation gives MAS glasses a brown colour which is darker with increasing MoO_3 additions. The cast MAS-0M to MAS-7M glasses are visually clear and transparent whereas MAS-8M glass is homogeneous as a melt but becomes partly crystallised on casting and cooling.

Glass compositions measured by EDS are presented in Table 1. The as-prepared MAS glasses contain increased contents of SiO_2 and Al_2O_3, presumably due to attack of the mullite crucible by the glass melt, and a lower content of MgO compared with the batched values. It is notable that the base glass composition has the greatest incorporation of additional SiO_2 and Al_2O_3 indicating that this melt is the most aggressive to the crucibles.

The relationship between the retained and the batched MoO_3 levels is plotted in Fig. 1. Comparing the batched and measured $[MoO_3]/[MgO]$ ratios (as $[MgO]$ is not directly affected by crucible corrosion, unlike $[SiO_2]$ and $[Al_2O_3]$) indicates that essentially all the MoO_3 is retained and thus the retained MoO_3 level exhibits a linear increase from MAS-0M to MAS-6M glasses, after which the retained MoO_3 level is essentially constant in going from the MAS-6M glass to the glassy part of the MAS-8M sample. The highest MoO_3 level is 5.34 mol% (i.e. 12.28 wt%) in MAS-7M glass. The density increases with MoO_3 addition from 2.696 g cm^{-3} for the MAS-0M glass to 2.782 g cm^{-3} for the MAS-7M glass (see Fig. 2); the density data can be fitted by a quadratic curve ($R^2 = 0.9963$). The density of MAS-8M glass being 2.790 g cm^{-3} also agrees well with the fitting curve even though this sample contains some crystalline material.

3.2. XRD, DTA and HT-XRD

The XRD patterns of all samples are shown in Fig. 3. Glasses with up to 6.54 mol% MoO_3 additions (MAS-0M to MAS-7M) are XRD amorphous with the XRD pattern displaying a hump between 20-50º (2θ). There are some small crystalline peaks superimposed on the diffuse scattering in the XRD pattern of MAS-8M glass, indicating the existence of crystalline phases in this glass. Using the ICDD database the crystalline phase was identified to be $MgMoO_4$ (PDF4 (2012), No.00-021-0961) although the existence of other minority phases, such as enstatite ($Mg_2Si_2O_6$), which we have seen when we loaded these glasses with Cl^-, cannot be definitively excluded.

Fig. 4 shows two typical DTA curves. MAS-0M to MAS-6M glasses have a curve like the black solid one whereas MAS-7M and MAS-8M glasses have a curve like the red dash one; the main difference is the disappearance of the second and sharp exothermic peak in the red dash curve. All the curves exhibit no features until the glass transition temperature (T_g) is reached, which is estimated from the onset of the first endothermic peak, suggesting the good thermal stability of the prepared glasses. There are two exothermic peaks recorded after T_g indicating two distinct crystallisation events upon heating. The relations between the temperatures at which the above thermal reactions occur and the molybdate addition in glass are plotted in Fig. 5. Both T_g and T_{c1} (first crystallisation temperature) exhibit similar downwards linear trends with increasing molybdate content, reducing from 775 ºC for MAS-0M to 741 ºC for MAS-8M and from 831 ºC for MAS-0M to 794 ºC for MAS-8M, respectively. T_{c2} (second crystallisation temperature) also exhibits a downwards linear trend reducing from 1010 ºC for MAS-0M to 923 ºC for MAS-6M glasses.

Figs. 6(a) - 6(d) present the high temperature XRD patterns of MAS-0M, MAS-3M, MAS-6M and MAS-7M glasses, respectively. The main phase after first glass crystallisation is cordierite ($Mg_2Al_4Si_5O_{18}$, PDF4 (2012), No.00-012-0303) which crystallises from the base glass network. Meanwhile, a number of relatively low intensity peaks assigned to $MgMoO_4$ (PDF4 (2012), No.00-021-0961) can be found in molybdate containing glasses at $2\theta = 22.6°$ (021), 25.0° (201), 26.8° (-112) and 33.2° (-312) and overlapping with peaks of cordierite at $2\theta = 18.7°$ (-201), 31.6° (-131), 36.0° (400) and 52.4° (151). In the temperature range 900 to 1000 °C, the peaks of $MgMoO_4$ appear and are intensified in the MAS-3M and MAS-6M glasses whereas in the MAS-7M glass the relative intensity does not change with increasing temperature. However, a peak at 25.7 °2θ appears at 950 °C and merges with the neighbouring peak at 26.0 °2θ at 1000 °C in the MAS-7M sample. In addition, the XRD patterns of MAS-0M glass indicate little change except a peak at 25.6 °2θ which vanishes between 900 and 1000 °C.

3.3. Raman spectra

Background subtraction of Raman spectra was conducted prior to detailed analysis. In the literature Raman background subtraction has been conducted using a variety of methods including piecewise linear functions [26], cubic splines [27] and quadratic functions [28]. In the current work it was found that the background in the interval between 1300 and 2000 cm^{-1}, where no Raman signal should be detected, was best fit using an exponential function and this was then used for background subtraction. Afterwards, the subtracted intensity was multiplied by the Long correction factor [29] which is dependent on frequency and temperature. Finally the corrected spectra were normalised by the highest intensity data in the 500 – 700 cm^{-1} band to enable comparison of bands assigned to molybdate with silicate bands.

The normalised Raman spectra of all samples are presented in Fig. 7. MAS-0M glass reveals two prominent broad bands centred at ~980 cm^{-1} and ~550 cm^{-1}, which are assigned to the vibrations of Si-O stretching modes and Si-O-Si bending modes in depolymerised structural units [30-31], respectively. Molybdate incorporation results in two new bands positioned at ~320 cm^{-1} and ~965 cm^{-1}, respectively. The 320 cm^{-1} band is a convolution of the symmetric and asymmetric bending vibration modes (v_2 and v_4) in MoO_4^{2-} tetrahedra while the 965 cm^{-1} band is a convolution of the symmetric and asymmetric stretching vibration modes (v_1 and v_3) in MoO_4^{2-} tetrahedra. The vibration frequencies of MoO_4^{2-} tetrahedra are given in [32] and [33] for alkali and alkaline earth molybdate crystals. In amorphous materials such as glass, the variable local environments means that only two broad bands are attained. No band assigned to reduced molybdenum (at 750-850 cm^{-1}, according to [34]) has been observed. In the crystallised region of MAS-8M sample, these two bands are split into a number of sharp peaks which prove the existence of a crystalline molybdate phase.

The significant overlapping of the 965 cm^{-1} molybdate band and 980 cm^{-1} silicate band makes it difficult to carry out reliable deconvolution of the primary band observed between 900 and 1200 cm^{-1} to identify the Q-speciation of the glasses. However, the areas of the molybdate bands can be compared with the area of the silicate band at 550 cm^{-1} which does not overlap with any band assigned to MoO_4^{2-}. Assuming that the area ratio of the 980 cm^{-1} silicate band to the 550 cm^{-1} silicate band is constant among all of the MAS glasses, then the area of the silicate band at 980 cm^{-1} can be estimated from the area of the silicate band at 550 cm^{-1} assuming that there is no major change in glass polymerisation across the compositions studied. This assumption is reasonable for these

glasses given that the [Al]/[Si] ratio and the [modifier]/([Al]+[Si]) ratios are essentially constant, unless Mo is acting as a modifier; previous work indicates that although Mo associates with modifiers it does not act as a modifier [35]. Hence the area of the 965 cm^{-1} molybdate band can obtained by subtracting the area of the estimated 980 cm^{-1} silicate band from the whole area of this region. Meanwhile, the area of 320 cm^{-1} the molybdate band can be directly obtained by comparison with the area of 550 cm^{-1} silicate band. The relative values for these areas are plotted in Fig. 8 as a function of molybdate addition. It is obvious that, as for both molybdate bands, the relative area increases linearly with molybdate additions, reaches maximum at MAS-6M glass and slightly reduces with further molybdate additions.

3.4. Microstructure

The backscattered SEM images (Fig.9) of MAS-4M glass appear featureless within the limit of resolution, indicating the micro-homogeneity of glass. Element distribution has been scanned over an area of 1600 µm^2 with Si Kα, Al Kα, Mg Kα and Mo Lα X-rays, as shown in Fig. 9, suggesting that all elements are distributed homogeneously within the glass matrix. The backscattered SEM images of MAS-8M glass are presented in Figs. 10a and 10b. Fig. 10a illustrates a boundary area between the two distinct regions of MAS-8M sample: a region which remains completely homogeneous, which is assumed to be glass, and a crystallised region where a large number of particles separated from the glass matrix can be observed. These two regions are separated by a boundary region made up of even smaller particles. Fig. 10b shows an area inside the crystallised part of the MAS-8M sample. The crystallised particles are spherical (droplet-like) and are randomly dispersed in this region. The diameters of these spheres are not constant, varying from 200 to 400 nm. EDS analysis (Table 1) indicates that the crystallised region of MAS-8M sample contains more Mg and Mo than the glassy region does; however, due to the resolution limit of EDS (1 µm), the exact composition of these spheres cannot be obtained.

Fig. 11 exhibits a TEM image of some pieces of the crystallised part of MAS-8M glass, along with electron diffraction patterns of selected areas. The separated crystals (Area C) have a distinctive morphology compared to the glass matrix (Areas A and B) under TEM; the electron diffraction patterns for Areas A and B are composed of scattered weak rings with a small amount of bright diffraction rings (Figs. 11A and 11B), indicating the predominant amorphous nature of these areas. Diffraction patterns for Area C consist of numerous bright diffraction rings and spots (Fig. 11C), which means multiple crystals are dominant in Area C. Fig. 11D primarily consists of two series of diffraction spots, indicative of [101] and [201] diffraction axes of single monoclinic MgMoO$_4$ crystals, respectively.

4. Discussion

4.1. Capacity of MAS glass to incorporate molybdate

The prepared MAS glasses have an excellent capacity for the incorporation and retention of MO_3 compared with previously reported silicate glass systems [10-11, 13-17, 36]. The occurrence of molybdate crystallisation in MAS-8M glass indicates that the loading limit of MoO_3 in MAS glass is reached at around 5.3 mol% (MAS-7M). This is much higher than that reported for borosilicate glasses or in related alkaline earth aluminosilicate glasses ($45SiO_2$-$10Al_2O_3$-$45MO$, mol%, M = Mg, Ca, Sr, Ba, Mg+Ca (1:1) or Sr+Ba (1:1)), as shown in Fig. 12. It is also notable in Fig 12 that in calcium-magnesium aluminosilicate glasses the solubility limit is in line with that found in calcium aluminosilicate glass, implying that MoO_4^{2-} ions tend to separate from the glass network with Ca^{2+} ions rather than Mg^{2+} ions whenever possible. Thus the MoO_3 solubility in glass seems to be controlled by the molybdate compound with the highest crystallisation tendency.

However, the retention results (Fig. 1) indicate that the incorporated MoO_3 level is essentially constant from glass MAS-6M onwards, showing that the saturation limit molybdate incorporation into the glass network is being reached. Such a MoO_3 saturation in MAS glass is also reflected by the relative area of molybdate bands to silicate bands in Raman spectra. The minor differences in relative areas among samples MAS-6M to MAS-8M (glassy part) glasses suggest that there is limited structural change among them. As the amount of excess molybdate becomes greater phase separation can occur in the final product (MAS-8M).

4.2. Effects of molybdate incorporation on MAS glass structure and properties

The increase in density with molybdate incorporation is a consequence of the greater mass of MoO_3 compared to the other components. Molybdate retention shows a linear increase from 0 to ~5.3 mol% MoO_3 addition while the density increase follows a quadratic dependency on MoO_3 addition (Fig. 2). This discrepancy may suggest that the addition of MoO_3 leads to an expansion in the glass network.

The linear decrease in T_g with increasing molybdate incorporation does not agree with the assumption that MoO_4^{2-} ions are only associated with Mg^{2+} ions which originally function as the only network modifiers in MAS glass. In that case, the polymerisation of the glass network would be increased resulting in an increased T_g. The decrease in T_g probably results from the association of MoO_4^{2-} ions with some Mg^{2+} ions which originally function as a charge compensator of AlO_4^- tetrahedra. This association depolymerises the aluminosilicate glass network and leads to a T_g decrease. It seems likely that this has a stronger effect on T_g than the association of MoO_4^{2-} ions with network modifiers Mg^{2+} and as a result T_g reduces with increasing molybdate incorporation.

There is little change in the XRD patterns of MAS-0M to MAS-6M glasses from 900 to 1000 °C (Fig. 6); however, an intense exothermic peak can be observed in the temperature range in their DTA curves (Fig. 4). This crystallisation peak may be attributed to the transition between cordierite and indialite phases at high temperature (cordierite and indialite crystals have similar structures and thus their XRD patterns are closely related [37-38]). Nevertheless, this transition does not occur in MAS-7M and MAS-8M glasses and therefore that peak does not appear in their DTA curves (Fig. 4). Moreover, in MAS-7M glass, the intensities of the $MgMoO_4$ diffraction peaks do not increase with temperature, indicating that $MgMoO_4$ has finished crystallisation

simultaneously with cordierite/indialite. The emergence of a peak at $2\theta = 25.7°$ at 950 °C in MAS-7M glass, in accordance with the small exothermic peak in DTA curve, is probably due to the occurrence of a reversible cordierite to mullite phase change at high temperatures [39].

The incorporation of molybdate leads to significant changes in the Raman spectra. The linear increase in the relative areas of molybdate bands (at 320 cm^{-1} and 965 cm^{-1}) to silicate bands (at ~980 cm^{-1}) from MAS-0M to MAS-6M glass is caused by the increasing number of MoO_4^{2-} tetrahedra dissolved in glass; no consistent variation in peak position with Mo content is observed however. The relative similarity in values in going from the MAS-6M to MAS-8M glasses reflects molybdate saturation in the glass network.

4.3. Phase separation of excess molybdate in MAS glasses

The excess molybdate which cannot enter the glass network separates from the melt during cooling, as observed in the MAS-8M sample (Fig. 10). XRD patterns (Fig. 3) indicate that the separated phase is most likely to be $MgMoO_4$, although the number of clearly corresponding peaks is limited. Raman spectra (Fig. 7) also show the dominance of $MgMoO_4$ in separated phase from the comparison with the spectrum of $MgMoO_4$ crystals.

SEM images (Fig. 10) show the formation of droplet-like particles within MAS-8M glass. These randomly distributed particles are all spherical and have a clear interface with the glass matrix. Phase separation is more likely to occur through liquid-liquid separation in the melt rather than the direct nucleation from saturated melt during cooling. The separated phase exhibits a strong crystallisation tendency and eventually each particle is made up of numerous single $MgMoO_4$ crystals. The wasteform produced at excess molybdate content resembles the French glass composite material (GCM) termed U-Mo glass which is formed by cold crucible melting that partly crystallises on cooling [29]. GCMs wasteform can be a useful compromise between glasses and ceramics, being easier and less expensive to prepare than conventional ceramics, but offering higher durability than glasses [40-41]. This is the approach adopted to date in France for waste with high MoO_3 content [2, 14]. Nevertheless, the glasses developed here represent an alternative approach in that promote high MoO_3 solubility in a fully vitreous wasteform.

Conclusions

MAS glasses with significant MoO_3 additions have been successfully prepared and the following conclusions can be drawn.

1) The capacity of MAS glass to accommodate molybdate found in this work is ~5.3 mol% (12.3 wt%) MoO_3. Saturation of molybdate is demonstrated both by compositional analysis and the relative areas of molybdate bands to silicate bands in Raman spectra becoming constant for glasses MAS-6M, MAS-7M and the glassy part of MAS-8M.
2) Increasing the MoO_3 content results in a quadratic increase in glass density.
3) The incorporated molybdate is thermally stable in glass until other phases start to form on heating. Molybdate incorporation linearly decreases glass transition and crystallisation temperatures. High temperature XRD patterns indicate that magnesium molybdate ($MgMoO_4$) crystallises either after or simultaneously with the formation of cordierite at a temperature above T_g upon heating. Further work is required to determine whether the two crystallisation events are linked or otherwise.
4) MAS-8M glass appears partly crystallised. Phase separation occurs due to the excess molybdate being expelled from the melt on cooling, resulting in the formation of droplet-like $MgMoO_4$ particles which are 200-400 nm in diameter and randomly dispersed within the glass matrix.

References

[1]	B. F. Dunnett, N. R. Gribble, R. J. Short, E. Turner, C. J. Steele, A. D. Riley, Glass Technol.: Eur. J. Glass Sci. Technol., Part A, 2012, 54 (3), 166-171.

[2]	R. Do Quang, V. Petitjean, F. Hollebecque, O. Pinet, O. Flament, A. Prod'homme, WM'03 Conference, Tucson, AZ, 2003.

[3]	W. Lutze, R. C. Ewing, Radioactive Wasteforms for the Future. North Holland: Amsterdam, 1988.

[4]	M. I. Ojovan, W. E. Lee, An Introduction to Nuclear Waste Immobilisation. Elsevier: Amsterdam, 2005.

[5]	R. J. Short. Incorporation of molybdenum in nuclear waste glasses. PhD Thesis, the University of Sheffield, UK, 2004.

[6]	R. J. Short, R. J. Hand, N. C. Hyatt, G. Mobus, J. Nucl. Mater., 2005, 340 (2-3), 179-186.

[7]	T. Taurines, B. Boizot, J. Non-Cryst. Solids, 2011, 357 (14), 2723-2725.

[8]	N. C. Hyatt, R. J. Short, R. J. Hand, W. E. Lee, F. Livens, J. M. Charnock, R. L. Bilsborrow, Chapter in Environmental Issues and Waste Management Technologies in the Ceramic and Nuclear Industries X, John Wiley & Sons, Inc.: 2006, 179-187.

[9]   L. Galoisy, L. Cormier, S. Rossano, A. Ramos, G. Calas, P. Gaskell, M. Le Grand, Mineral. Mag., 2000, 64 (3), 409-424.

[10]   F. Farges, R. Siewert, G. E. Brown, A. Guesdon, G. Morin, Can. Mineral., 2006, 44, 731-753.

[11]   G. Calas, M. Le Grand, L. Galoisy, D. Ghaleb, J. Nucl. Mater., 2003, 322 (1), 15-20.

[12]   N. C. Hyatt, R. J. Short, R. J. Hand, W. E. Lee, F. Livens, J. M. Charnock, R. L. Bilsborrow, Chapter in Environmental Issues and Waste Management Technologies in the Ceramic and Nuclear Industries, 2012, 179-185.

[13]   D. Caurant, O. Majerus, E. Fadel, A. Quintas, C. Gervais, T. Charpentier, D. Neuville, J. Nucl. Mater., 2010, 396 (1), 94-101.

[14]   D. Caurant, O. Majérus, E. Fadel, M. Lenoir, C. Gervais, O. Pinet, J. Am. Ceram. Soc., 2007, 90 (3), 774-783.

[15]   S. Schuller, O. Pinet, A. Grandjean, T. Blisson, J. Non-Cryst. Solids, 2008, 354 (2-9), 296-300.

[16]   N. Chouard, D. Caurant, O. Majerus, J. L. Dussossoy, A. Ledieu, S. Peuget, R. Baddour-Hadjean, J. P. Pereira-Ramos, J. Non-Cryst. Solids, 2011, 357 (14), 2752-2762.

[17]   M. Magnin, S. Schuller, C. Mercier, J. Trébosc, D. Caurant, O. Majérus, F. Angéli, T. Charpentier, C. Jantzen, J. Am. Ceram. Soc., 2011, 94 (12), 4274-4282.

[18]   C. M. Jantzen, J. Non-Cryst. Solids, 1986, 84 (1-3), 215-225.

[19]   I. Techer, T. Advocat, J. Lancelot, J. M. Liotard, J. Nucl. Mater., 2000, 282 (1), 40-46.

[20]   I. Techer, T. Advocat, J. Lancelot, J. M. Liotard, Chem. Geol., 2001, 176 (1-4), 235-263.

[21]   G. Leturcq, G. Berger, T. Advocat, E. Vernaz, Chem. Geol., 1999, 160 (1-2), 39-62.

[22]   J. E. Shelby, J. Am. Ceram. Soc., 1985, 68 (3), 155-158.

[23]   M. Tiegel, A. Herrmann, C. Russel, J. Korner, D. Klopfel, J. Hein, M. C. Kaluza, J. Mater. Chem. C, 2013, 1 (33), 5031-5039.

[24]   S. Siwadamrongpong, M. Koide, K. Matusita, J. Non-Cryst. Solids, 2004, 347 (1-3), 114-120.

[25]   J. Schofield. Vitrification of a chloride containing actinide waste surrogate. PhD Thesis, the University of Sheffield, UK, 2011.

[26]   S. J. Baek, A. Park, A. G. Shen, J. M. Hu, J. Raman Spectrosc., 2011, 42 (11), 1987-1993.

[27]   H. Behrens, J. Roux, D. R. Neuville, M. Siemann, Chem. Geol., 2006, 229 (1-3), 96-112.

[28]   V. P. Zakaznova-Herzog, W. J. Malfait, F. Herzog, W. E. Halter, J. Non-Cryst. Solids, 2007, 353 (44-46), 4015-4028.

[29]   D. A. Long, Raman spectroscopy. McGraw-Hill Inc.: London, 1977.

[30]   D. R. Neuville, B. O. Mysen, Geochim. Cosmochim. Acta, 1996, 60 (10), 1727-1737.

[31]   P. F. Mcmillan, Annu. Rev. Earth. Pl. Sc., 1989, 17, 255-283.

[32]   G. D. Saraiva, W. Paraguassu, M. Maczka, P. T. C. Freire, J. A. Lima, C. W. A. Paschoal, J. Mendes Filho, A. G. Souza Filho, J. Raman Spectrosc., 2008, 39 (7), 937-941.

[33]   T. Ozeki, K. Murata, H. Kihara, S. Hikime, Bull. Chem. Soc. Jpn., 1987, 1987 (60), 3585-3589.

[34]   E. Payen, J. Grimblot, S. Kasztelan, J. Phys. Chem., 1987, 91, 6642-6648.

[35]   P. Colomban, O. Paulsen, J. Am. Ceram. Soc., 2005, 88 (2), 390-395.

[36]   N. Henry, P. Deniard, S. Jobic, R. Brec, C. Fillet, F. Bart, A. Grandjean, O. Pinet, J. Non-Cryst. Solids, 2004, 333 (2), 199-205.

[37]   A. Miyashiro, Am. J. Sci., 1957, 255 (1), 43-62.

[38]   G. V. Gibbs, Am. Mineral., 1966, 51, 1068-1087.

[39]   S. M. Logivinkov, G. D. Semchenko, D. A. Kobyzeva, Refract. Ind. Ceram., 1996, 37 (11-12), 378-381.

[40]   W. E. Lee, M. I. Ojovan, M. C. Stennett, N. C. Hyatt, Adv. Appl. Ceram., 2006, 105 (1), 3-12.

[41]   C. M. Jantzen, W. E. Lee, M. I. Ojovan, Chapter 6 in Radioactive waste management and contaminated site clean-up: Processes, technologies and international experience, W. E. Lee; M. I. Ojovan; C. M. Jantzen, Eds. Woodhead: Cambridge, 2013, 171-272.

Tables and Figures.

Table 1. Nominal and measured glass composition (mol%).

Sample	SiO_2		Al_2O_3		MgO		MoO_3	
	Batched	Measured	Batched	Measured	Batched	Measured	Batched	Measured
MAS-0M	45.00	50.06	10.00	14.63	45.00	35.31	0	0
MAS-1M	44.55	46.99	9.90	11.49	44.55	40.58	0.99	0.94
MAS-2M	44.12	46.57	9.80	11.69	44.12	39.95	1.96	1.78
MAS-3M	43.69	46.24	9.71	11.82	43.69	39.18	2.91	2.76
MAS-4M	43.27	46.01	9.62	11.91	43.27	38.38	3.85	3.71
MAS-5M	42.86	46.07	9.52	12.13	42.86	37.34	4.76	4.46
MAS-6M	42.45	46.33	9.43	12.49	42.45	36.02	5.66	5.16
MAS-7M	42.06	46.10	9.35	12.36	42.06	36.21	6.54	5.34
MAS-8M	41.67	46.84	9.26	12.72	41.67	35.14	7.41	5.30
MAS-8M(C)	-	43.77	-	11.93	-	36.48	-	7.81
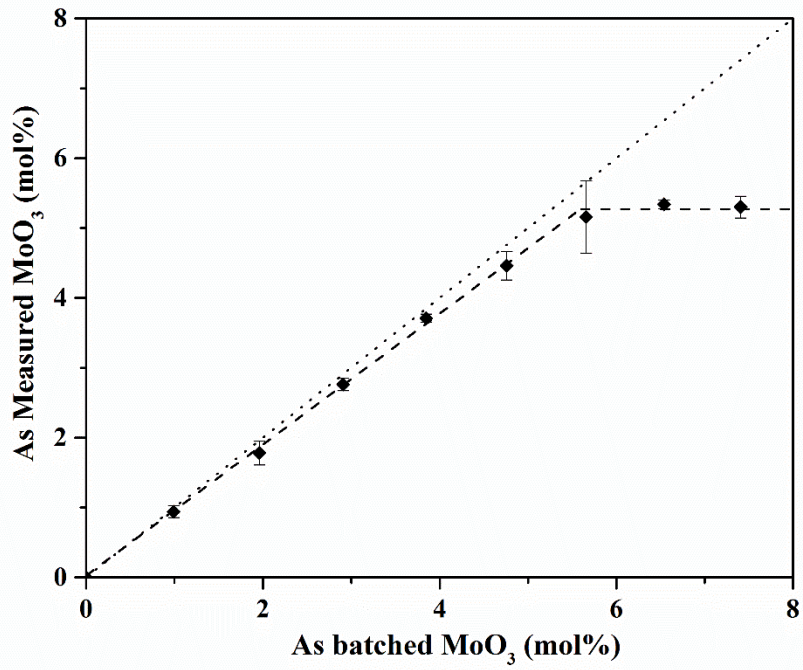
Fig.1. Correlation between the measured and the batched MoO_3 levels in MAS glasses
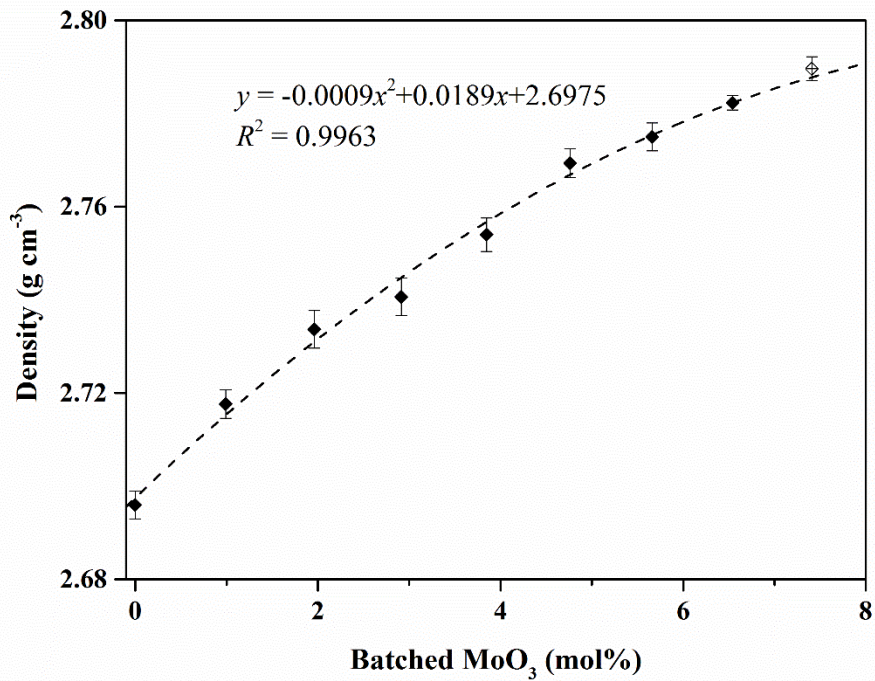
Fig. 2. Density change with increasing MoO_3 addition in MAS glasses.
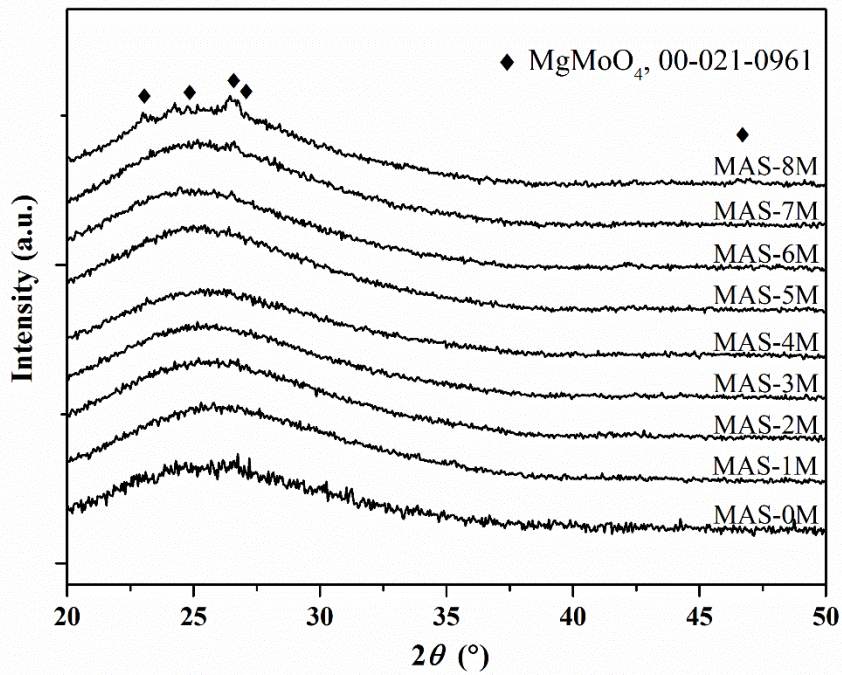
Fig. 3. XRD patterns of all MAS glasses ($45SiO_2$-$10Al_2O_3$-$45MgO$ with x mol% MoO_3 addition).
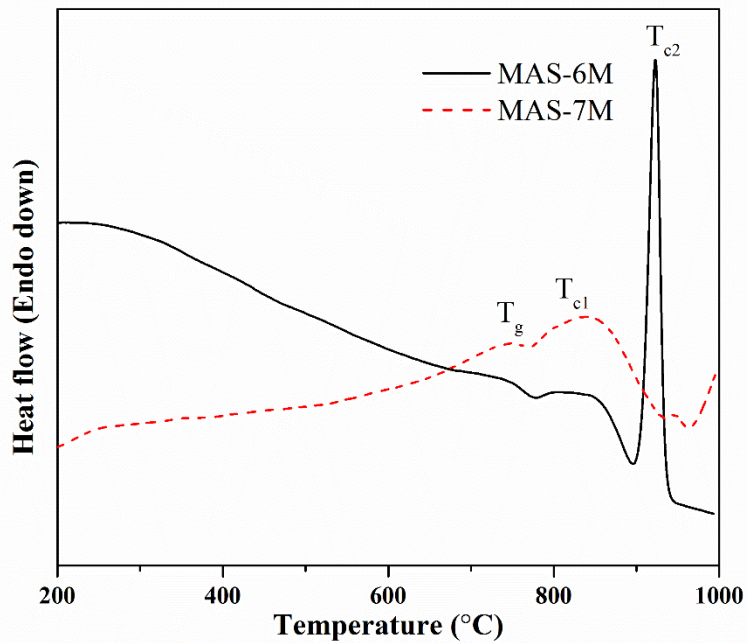
Fig. 4. Typical DTA curves. Curves of glasses MAS-0M to MAS-6M are like the black one while curves of samples MAS-7M and MAS-8M are like the red one.
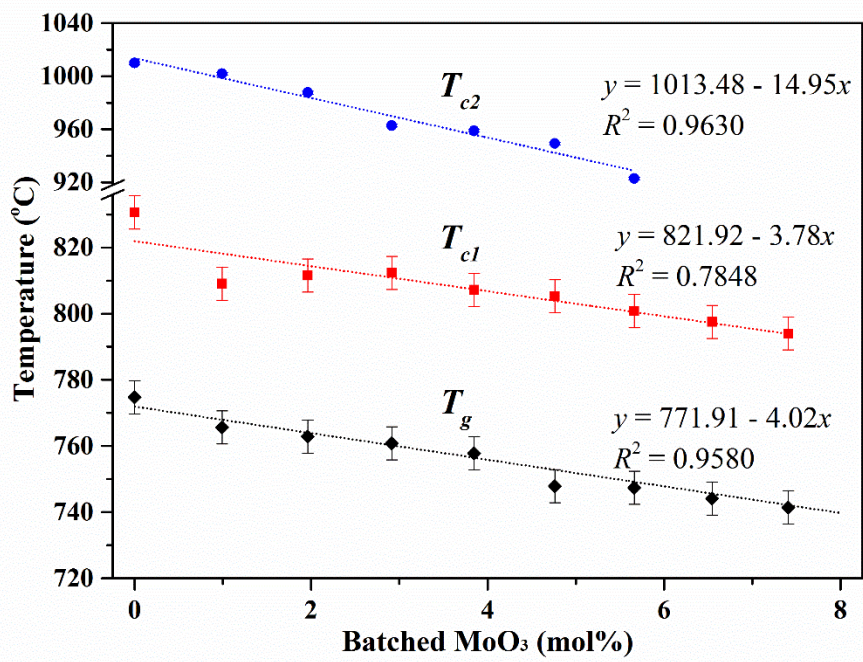
Fig. 5. Changes in T_g, T_{c1} and T_{c2} of MAS glass with increasing MoO_3 addition.
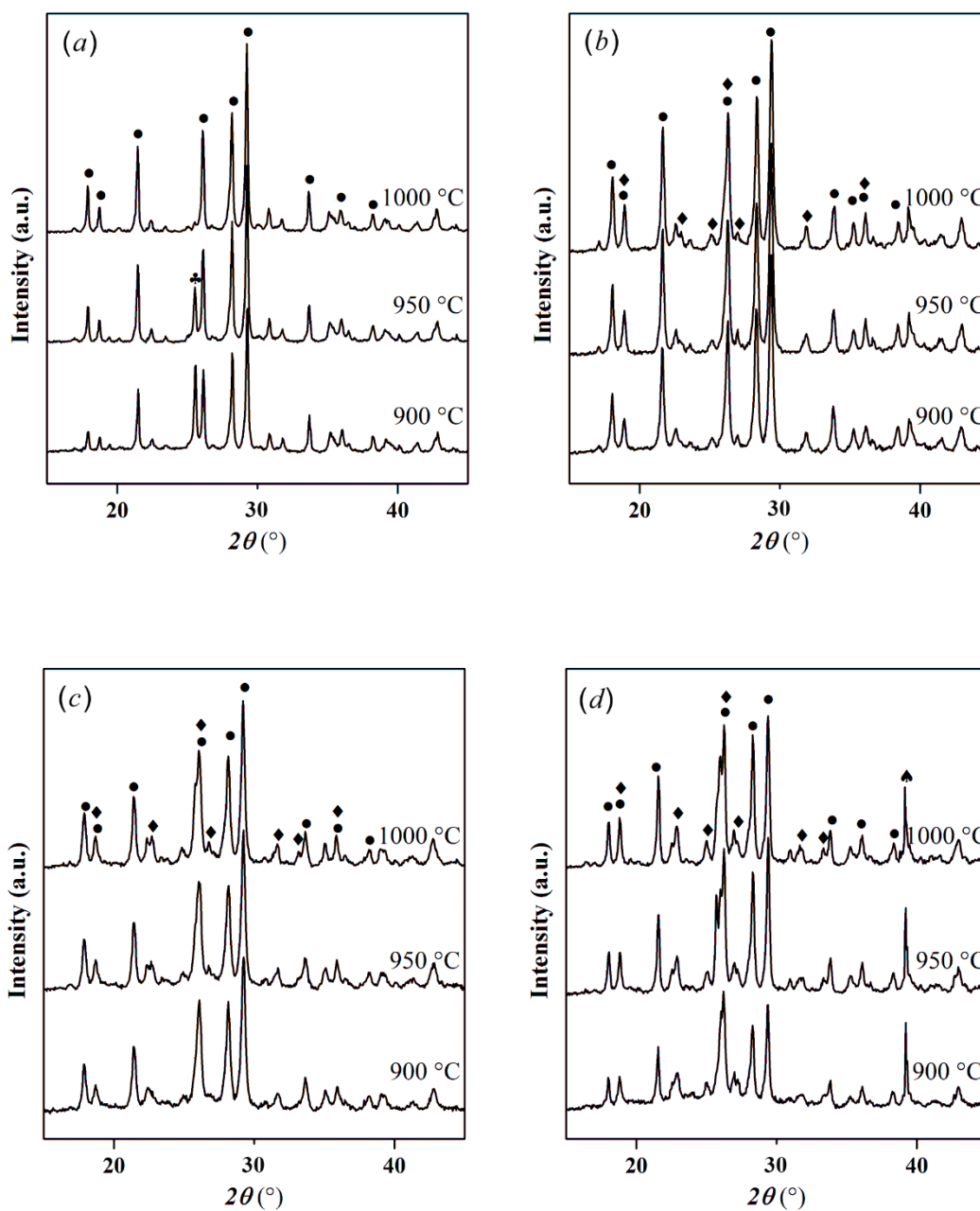
Fig. 6. High temperature XRD patterns of (a) MAS-0M, (b) MAS-3M, (c) MAS-6M and (d) MAS-7M. ($\bullet$ - cordierite/indialite $Mg_2Al_4Si_5O_{18}$, PDF4 (2012) No.00-012-0303/00-013-0293; $\clubsuit$ - metastable $Mg_2Al_4Si_5O_{18}$ at 900 °C, PDF4 (2012) No.00-014-0249; $\blacklozenge$ - $MgMoO_4$, PDF4 (2012) No.00-021-0961; $\spadesuit$ - platinum sample holder)
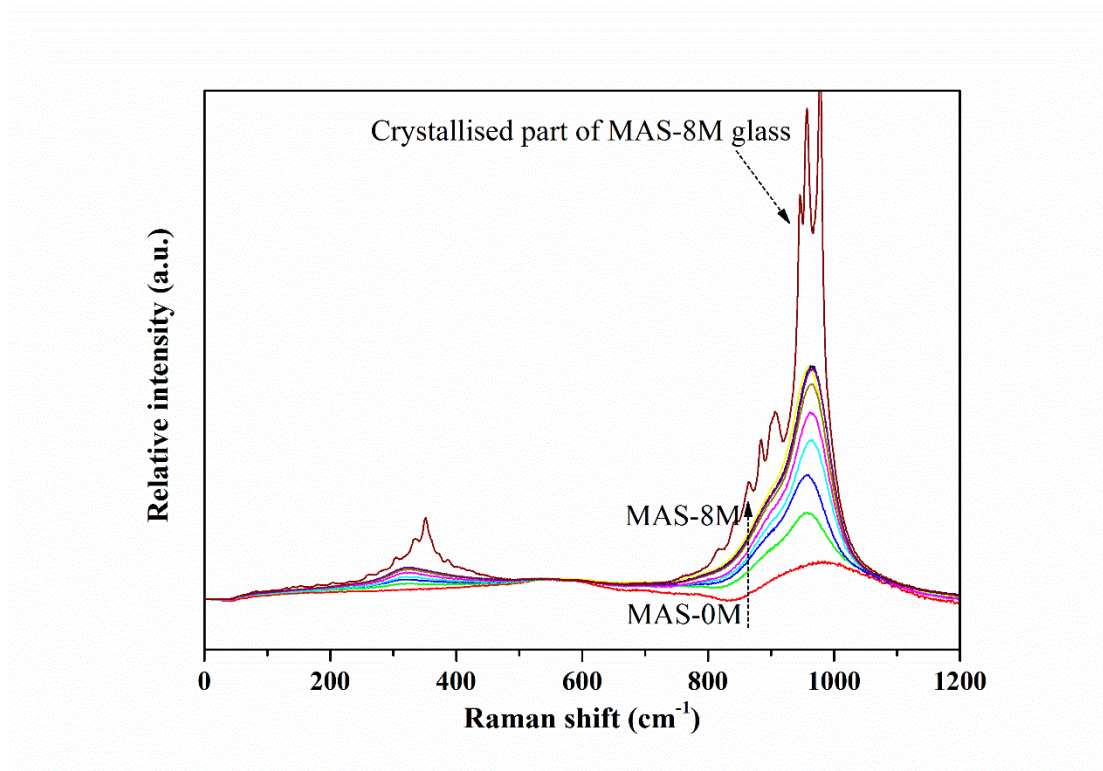
Fig. 7. Corrected Raman spectra of MAS-0M to MAS-8M glasses. For details of corrections used see main text.
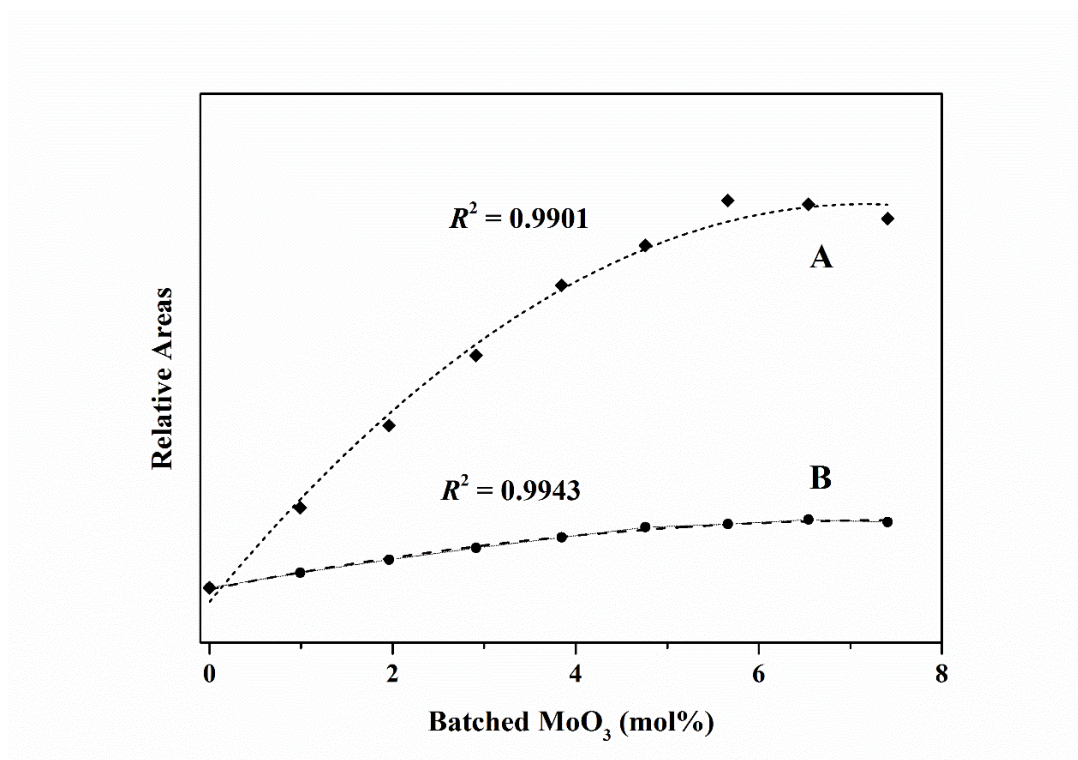
Fig. 8. Relative areas of the (A) estimated 980 cm^{-1} molybdate band and (B) 340 cm^{-1} molybdate band to 550 cm^{-1} silicate band. The curves are quadratic fits to the data.
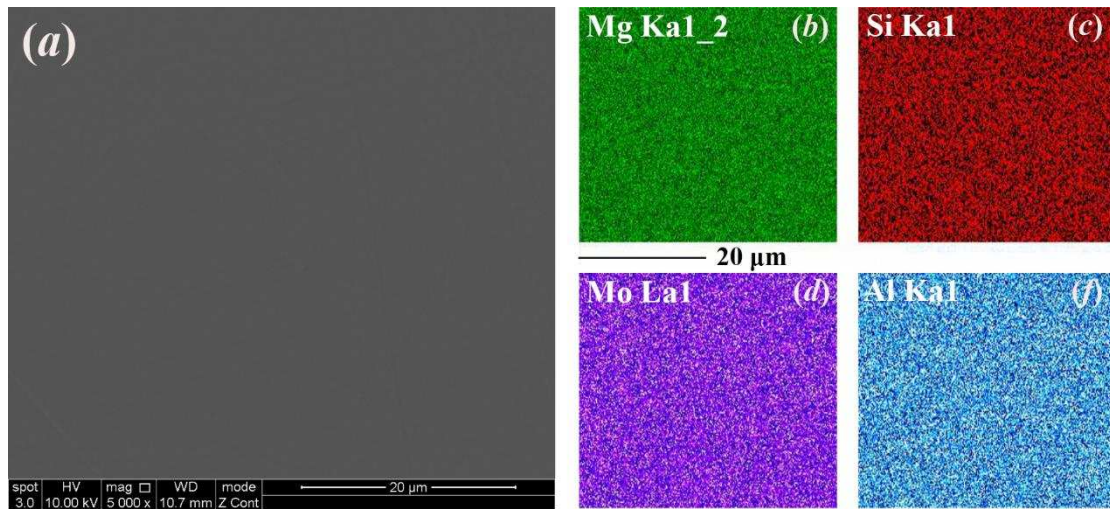
Fig. 9. (a) BEI of MAS-4M glass and (b-f) dot mapped elemental distribution within glass obtained by EDX.
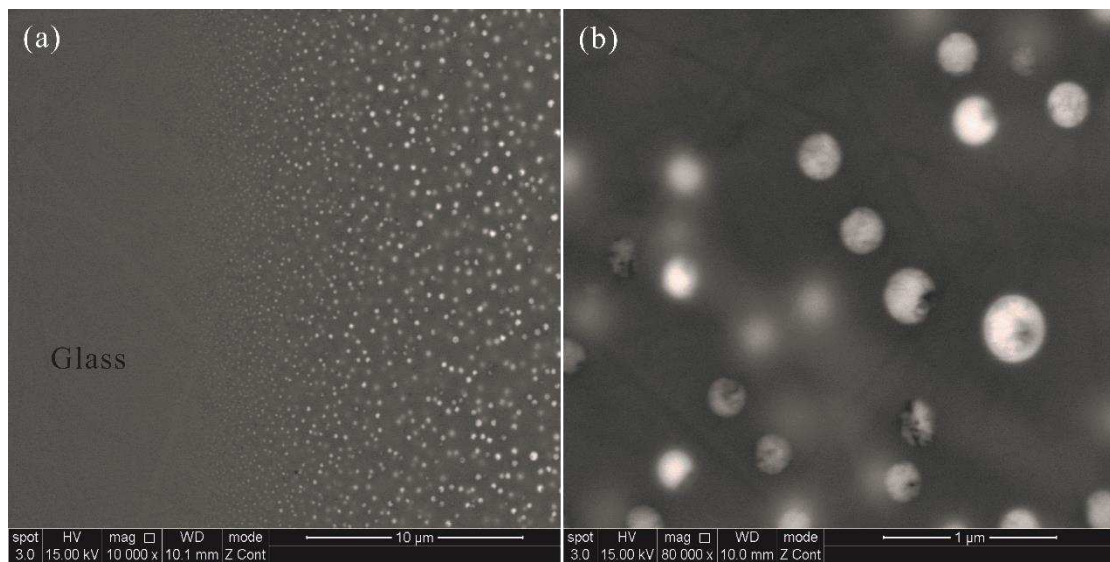
Fig. 10. SEM images (BEI) of MAS-8M: (a) boundary between the glassy region and crystallised region; (b) crystals within glass under high magnification.
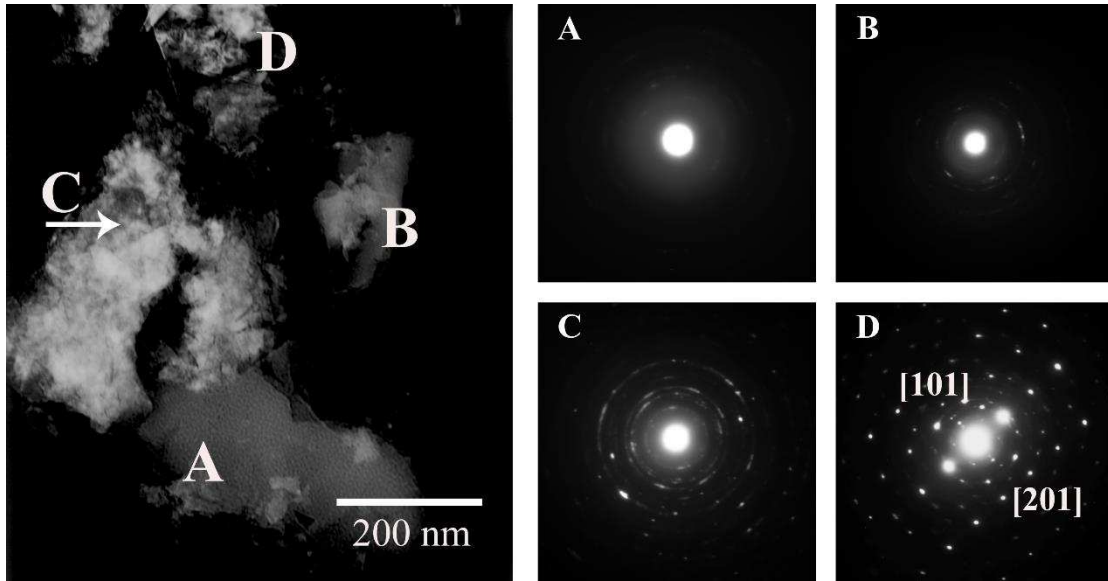
Fig. 11. TEM image showing crystallised material and glass matrix in the MAS-8M sample and the electron diffraction patterns of (A) glass matrix, (B) glass matrix with small amount of crystals, (C) crystallised area and (D) some single crystals.
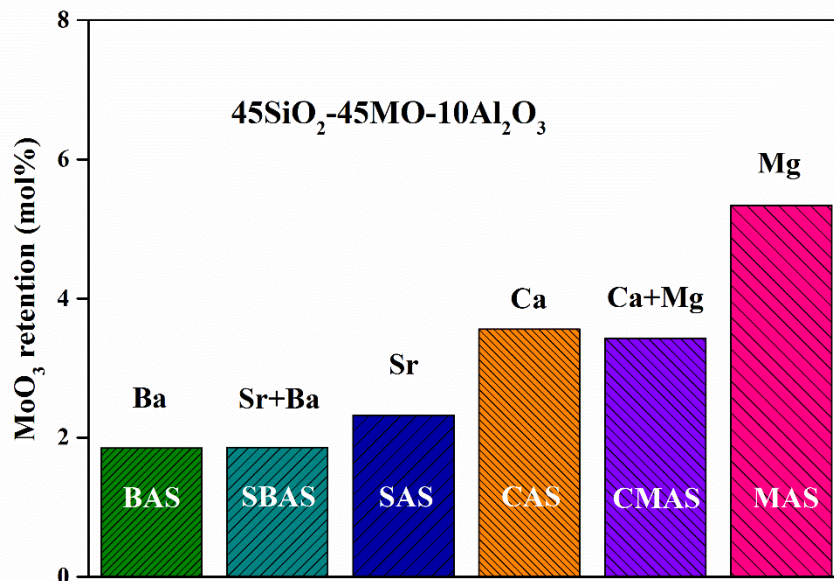
Figure 12. MoO$_3$ solubility limits in a range of 45AeO-10Al$_2$O$_3$-45SiO$_2$ glasses where Ae = Ba, (Sr:Ba), Sr, Ca, (Ca:Mg) and Mg (data for all glasses apart from the current Mg series taken from as yet unpublished results).